Effect of Breathing on UWB Propagation Characteristics for Ingestible and Implantable Devices

Concepcion Garcia-Pardo, Alejandro Fornes-Leal, Matteo Frasson,
Vicente Pons-Beltrán, Narcis Cardona

***Abstract*—Wireless in-body devices are those in which a medical sensor is introduced –implanted or ingested– inside the human body and communicates with a remote node. Some in-body applications demand high data rates are necessary, so Ultra-Wideband (UWB) spectrum has been proposed as a good candidate because of its large bandwidth available. Besides, breathing can lead to internal movement of the torso and consequently, of devices installed in this area. Thus, the radio channel performance can be affected by such movement leading to a malfunction of the radio interface of the medical device. This work aims at analyzing the effect of breathing on the propagation channel by means of *in vivo* measurements in living animal models. Continuous wave (CW) measurements have been carried out for five different frequencies in the lower part of the UWB band, and the effects of breathing on the relative received power (module and phase), are analyzed and discussed.**

***Index Terms*— *in vivo*, implant communications, in-body, UWB, breathing, path loss, antenna, wireless medical devices.**

I. Introduction

Wireless technologies have increased their presence in medical devices in the last years [1]. The advances in microelectronics have made possible the integration of biomedical sensors and radio transceivers in one single device. This is much more relevant for in-body devices, in which the medical sensor is implanted inside the body [2] or it has been ingested by the patient [3]. Cardiac implants such as pacemakers [4], electromyogram (EMG) sensors for controlling prostheses [5], or wireless capsule endoscopy (WCE) [6] are good examples of this kind of devices.

The IEEE Standard 802.15.6-2012 for Wireless Body Area Networks (WBAN) allocated initially the Medical Implant Communication Service (MICS) band, which operates from 402 to 405 MHz, for communications between an in-body sensor and another sensor located either inside, over or out of the body surface [7]. However, this band does not provide enough bandwidth to develop high data rate communications (e.g., high quality video transmission for WCE) [8]. The Industrial, Scientific and Medical (ISM) radio band (2400-2483.5 MHz) has been also explored for this purpose. Nevertheless, the overload of this frequency band hinders the implementation of medical communications on it [9]. Thus, Ultra-Wideband (UWB) frequency band (3.1-10.6 GHz) has been investigated in the last years as a candidate to be used on in-body communications due to its multiple advantages such as large bandwidth, low power consumption, or miniaturization capabilities [10], [11]. The main drawback of UWB for in-body communications is the large attenuation suffered by the transmitted signal due to: 1) the dielectric properties (dielectric constant and conductivity) of human body tissues, and 2) the frequency dependency of these properties [12], [13]. This makes that relative received power is frequency-dependent, so the characterization of the propagation channel [14] is much more challenging. Thus, most of the works focus on the lower part of the UWB spectrum [15] for implant or ingestible communications.

In literature, there are a wide variety of works analyzing propagation characteristics for implanted [15], [16] or ingestible devices [17], [18] either for UWB or other frequency bands. Results are highly dependent on the transmitting and receiving antennas used, the distance range considered, or the methodology of analysis selected (simulations, phantom experiments or *in vivo* measurements) [14], [17]. All these studies perform their analysis assuming a static radio channel, so that the path loss and other parameters can be directly deduced. However, since, in reality, the patient is continuously breathing, movement among internal organs is produced, especially in the torso area. This movement leads to relative displacement among the in-body device and the remote node, and consequently to changes in the propagation channel with time.

To the best of the authors' knowledge, the influence of the movement of the in-body antenna on the propagation channel is barely investigated in literature. The only work dealing with this issue is [19], where authors analyse the effect of breathing in Doppler characteristics for implant applications by performing measurements in a single-layer muscle phantom. The rest of works found in literature only consider applications in which the antennas are out of the body either over the surface (on-body) or away (off-body) [20]–[22]. Some other works have studied the effect of the natural movement of the organs in the propagation channel by modelling the movement in a software tool, which is not fully realistic [23].

This work aims at filling that gap analyzing the variation of the UWB propagation with time due to breathing. To accomplish this task, software simulations or laboratory measurements with phantoms are not good options since they cannot properly replicate the movement of the organs and antennas. Therefore, the most realistic and reliable way to simulate the human breathing is by *in vivo* measurements. Thus, in this paper, continuous wave (CW) measurements have been performed at different frequencies in the 3.1-5.1 GHz frequency band. The variation with time of the relative received power (module and phase) is evaluated and modeled.

The rest of the paper is organized as follows: Section II details the measurement methodology, animal preparation and the scenario considered; Section II analyzes and models the influence of breathing in the relative received power (module and phase); implications of such variation on real applications are discussed in Section IV. Finally, the main conclusions derived from this work are outlined in Section V.

This work was supported in part by the Ministerio de Ciencia e Innovación RTI2018-099880-B-C31; and in part by the Vicerrectorado de Investigación, Innovación y Transferencia de la Universitat Politècnica de València under COLODEM project (PAID-06-18 First Research Projects).

C. Garcia-Pardo, A. Fornes-Leal, and N. Cardona are with the iTEAM research institute, Universitat Politècnica de València, 46022 Valencia, Spain (e-mail: cgpardo@iteam.upv.es).

V.Pons-Beltrán, and M. Frasson are with the Digestive Diseases Area, Hospital Universitari i Politècnic La Fe, IIS La Fe, Valencia, 46026, Spain.

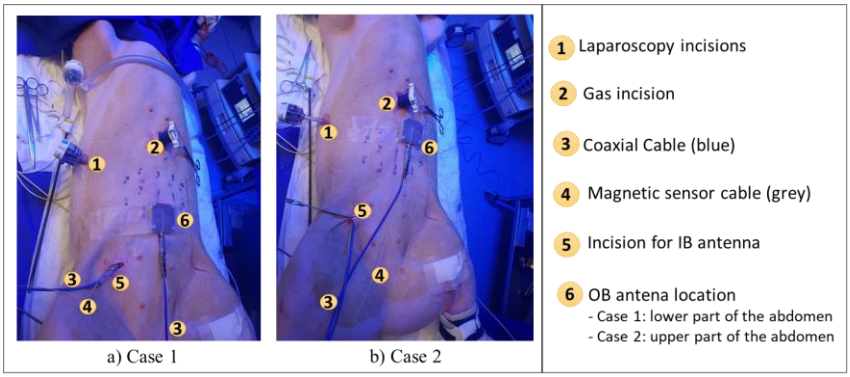

Fig. 1. *In vivo* measurement setup, medical instruments and antennas used for the two in-body configurations measured.

II. Methodology

A. Scenario

The scenario of application in this work is the in-body to on-body (IB2OB) configuration in which the implanted antenna is located inside the human body and the remote node is an antenna placed over the surface of the body. In this scenario, WCE (ingested device) in the gastrointestinal area, and cardiac devices (implanted device) in the chest area are two of the most known in-body applications.

Our analysis was particularized to the gastrointestinal area, where a WCE could be transmitting information from the small bowel to a remote receiver installed at patient's waist. In this case, the dielectric properties of the small bowel, fat and skin are the most dominant in terms of influence on the propagation channel [17]. This scenario was selected due to its simplicity for animal surgery compared to other parts of the human torso. For cardiac devices installed in the chest area, the tissues present in the propagation medium are similar compared to those of the gastrointestinal area. This is due to the fact that either colon or heart tissue are both tissues with a high content of water whereas fat and skin layer are present in both scenarios.

B. Measurement Setup

1) Animal Preparation

The *in vivo* experiment was prepared in accordance with the animal-care guidelines set forth by the national government and the European Commission, and then it was approved by the corresponding ethical committees of both the regional and the hospital authorities. It was carried out in an operating surgery room – restricted to research experiments– of Hospital La Fe, at a constant temperature of 21 ºC during the whole procedure. A porcine model of around 50 kg was considered as a test subject, due to its similarity to humans in terms of the size and distribution of its gastrointestinal organs. The arrangement of the animal as well as the instrumentation used in the experiment is depicted in Fig.1.

The animal preparation, whose procedure was conducted by surgeons, consisted of the following steps. First of all, the animal was sedated and anesthetized, condition that was kept during the whole trial. The animal's heart rate, blood pressure, respiratory frequency, and palpebral reflex were continuously monitored to correct any excess or shortage of anesthesia. The animal breathed in a relaxed manner in a rate of about 12-14 breaths per minute, which can be considered as a normal rate [22]. Then, a laparoscopy was performed in the abdominal cavity to insert the in-body antenna as can be seen in Fig. 1. To this end, four incisions were done: one for inserting the in-body antenna; another for inserting carbon dioxide (CO_2) to inflate the cavity to facilitate the positioning of the antenna; and two additional ones to insert the laparoscope and laparoscope tools (e.g., graspers) for seamlessly placing the antenna. Once the laparoscopy was done, the in-body antenna was placed in the desired position. Next, the abdominal cavity was deflated before starting to measure, removing any kind of gas, thus having more realistic conditions. Once the experiment was finished, all the tools were removed and cleaned.

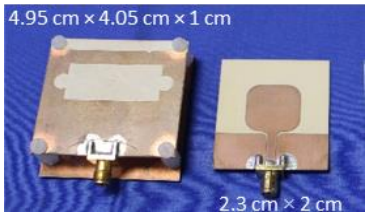

Fig. 2. On-Body (left) and In-Body (right) antennas.

2) Measurement Equipment and Antennas

Measurements were performed using the Keysight E5072A Vector Network Analyzer (VNA). The in-body (hereinafter denoted as IB) and on-body (hereinafter denoted as OB) antennas were connected to ports 1 and 2 of the VNA respectively by using 2-m-length coaxial cables and the required connectors. A laptop connected to the VNA was used to gather and store the measurements, using a custom application for automatizing the processes of calibration, measurement and data storage.

In Fig. 2, the antennas used are shown. The IB antenna is a patch antenna with a quasi-omnidirectional radiation pattern in the UWB frequency band. It was designed and miniaturized taking into account the operation environment and the surrounding tissues of the gastrointestinal area. More details about the IB antenna are given in [24]. Regarding the OB antenna, it is a slotted patch antenna which works in the lower part of the UWB frequency band. This antenna, was specially developed to be used over the surface of the body in the abdominal area. It was designed to optimize the penetration of the EM signal towards the inner of the body as well as to minimize the signals coming from the external environment. In [25], more details about this antenna are provided.

Besides, in order to know the real distance between both antennas with enough precision, a 3D magnetic tracker (trakSTAR, from Ascension Technology Corporation) was used, attaching a magnetic sensor to each antenna (see Fig. 1).

C. Methodology

The forward transmission (S_{21}) and reflection coefficients (S_{11}, S_{22}) of the antennas were measured by the VNA, which was configured in CW (continuous wave) mode. The VNA was programmed to characterize subsequently 5 specific frequencies of the UWB range, in particular 3.1, 3.6, 4.1, 4.6 and 5.1 GHz, in zero-span mode (CW) with an output power of 8 dBm. For each of them, N=2001 samples were taken during T=100 seconds, having a temporal resolution of 0.05 s, small enough to allow observing the effect of breathing on both the S_{21}, S_{11}, and S_{22}, parameters.

TABLE I
VARIATION OF THE DISTANCE BETWEEN ANTENNAS (CENTIMETERS)

	Case 1					Case 2				
	3.1 GHz	3.6 GHz	4.1 GHz	4.6 GHz	5.1 GHz	3.1 GHz	3.6 GHz	4.1 GHz	4.6 GHz	5.1 GHz
Mean	4,43	4,44	4,45	4,44	4,44	5,87	5,95	5,96	5,95	5,96
Max	4,53	4,54	4,56	4,53	4,56	6,12	6,16	6,15	6,15	6,16
Min	4,32	4,33	4,34	4,35	4,35	5,66	5,76	5,81	5,78	5,78
Std	0,03	0,03	0,03	0,03	0,03	0,08	0,07	0,06	0,06	0,06

After measurement configuration, but before inserting the antennas into the animal model, a full port calibration of the VNA was performed in order to remove the complex response of cables and connectors from measurements. Once calibrated, the antennas were connected to the VNA and the measurement procedure begun. The surgeon introduced the IB antenna through the incision (element 5 of Fig. 1), and then the position of the IB antenna was located in two different positions of the small bowel in order to evaluate the effect of breathing in different situations: i) Case 1: IB antenna located in the lower part of the abdomen, and ii) Case 2: IB antenna located in the upper part of the abdomen, near the thoracic cage. Such a precise control of the IB antenna position was achieved thanks to the laparoscopy technique. Regarding the OB antenna (element 6 of Fig. 1), it was oriented in parallel to the IB antenna, and placed over the skin of the animal's abdomen just above the IB one. This was accomplished by moving the OB antenna to the point where the distance among antennas given by the magnetic tracker was minimum.

III. RESULTS

From measurements, the S-parameters $S_{11}(t)$, $S_{22}(t)$, and $S_{21}(t)$, were recorded during T=100 seconds, being t the time vector with N=2001 points. As mentioned before, every S parameter was measured at 5 different frequencies f={3.1, 3.6, 4.1, 4.6, 5.1}×10^9 Hz, resulting in $S_{11}(f,t)$, $S_{22}(f,t)$, and $S_{21}(f,t)$.

Regarding distance between IB and OB antennas, d, it was measured continuously by the magnetic tracker during the entire measurement procedure. Thus, 3500 samples were recorded per frequency for every in-body position. Table 1 summarizes the statistics of the measured distance for every in-body position and every frequency under analysis. As it can be seen, the variation of the measured distance is much higher for Case 2, in which the antenna is nearer the thoracic cage, being the standard deviation more than twice that of the Case 1 configuration. Nevertheless, for both locations, the difference between maximum and minimum was below 0.5 cm.

A. Antenna Matching

The antenna matching parameter for the IB and OB atennas (S_{11} and S_{22} respectiverly) considering the two configurations (Case 1 and Case 2) and the five different frequencies measured is plotted in Fig. 3. Despite the breathing process, both the IB and the OB antennas are matched along the entire measurement time. Even though a slight ripple is observed in some cases, this does not affect their matching. Therefore, the correct operation of the antennas during the entire measurement procedure is confirmed.

B. Time-Varying Transfer Function

The time-varying transfer function T(f, t) for the set of frequencies f, can be directly deduced as T(f,t) = $S_{21}(f,t)$. From the time-varying transfer function, the time-varying relative received power for a particular frequency f_i, can be computed as $P_{rel}(t)$=20log$_{10}$(|T(t)|).

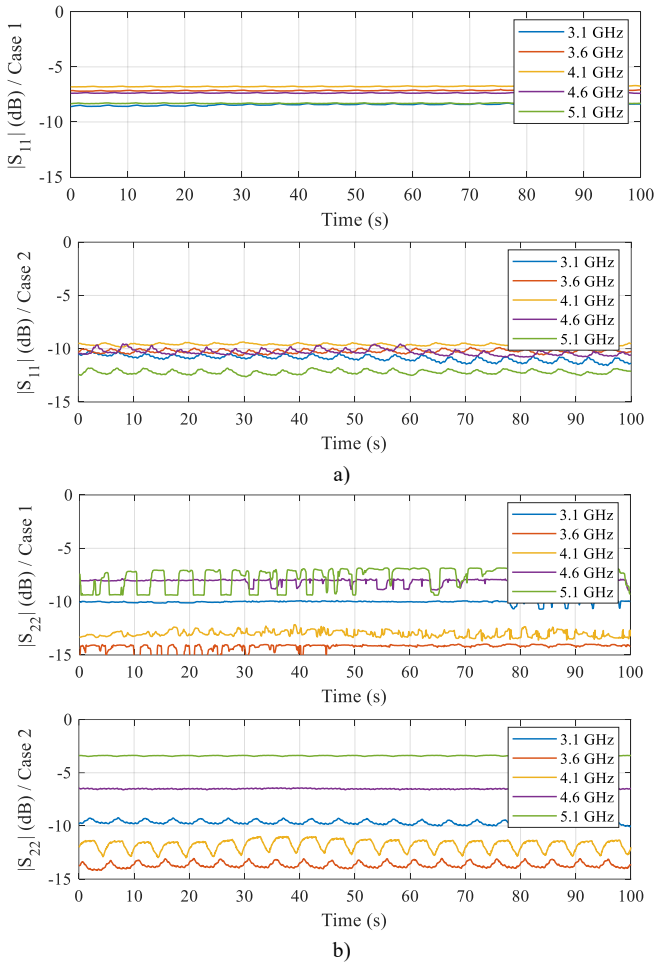

Fig. 3. Antenna matching for Case 1 and Case 2:
a) S_{11} (IB antenna), b) S_{22} (OB antenna).

1) Relative Received Power

Fig. 4 shows how the measured P_{rel} follows an oscillating behavior with time. Such oscillation is more pronounced for Case 2, in which both IB and OB antennas are closer to the thorax.

From measured data, two different fitting models are proposed:

- cosine model: $P_{rel}(t)$=A+Bcos(2πCt+D) and
- absolute value of the cosine: $P_{rel}(t)$=A+B|cos(2π(C/2)t+D)|

where, A is the mean relative received power in dB, B is the maximum excursion of the oscillating process, C is the breathing rate (breaths per second), t is the time vector, and D is the initial phase offset.

Table II shows shows the RMSE for the two models proposed, reporting a much lower error when fitting with the absolute value of the cosine. Thus, such model is the most appropriate for modeling P_{rel}. Fig. 4 shows in dashed black lines the model obtained for every frequency, while Table III reports the parameters A, B, C and D which provide the best fitting for the absoluete value of the cosine model.

TABLE II
RMSE FOR COSINE AN ABSOLUTE COSINE MODEL OF P_{REL}

	Case 1					Case 2				
	3.1 GHz	3.6 GHz	4.1 GHz	4.6 GHz	5.1 GHz	3.1 GHz	3.6 GHz	4.1 GHz	4.6 GHz	5.1 GHz
Cosine	0.24	0.10	0.12	0.18	0.31	0.37	1.20	1.06	1.44	0.81
Absolute cosine	0.14	0.10	0.09	0.11	0.27	0.26	1.01	1.00	0.64	0.77

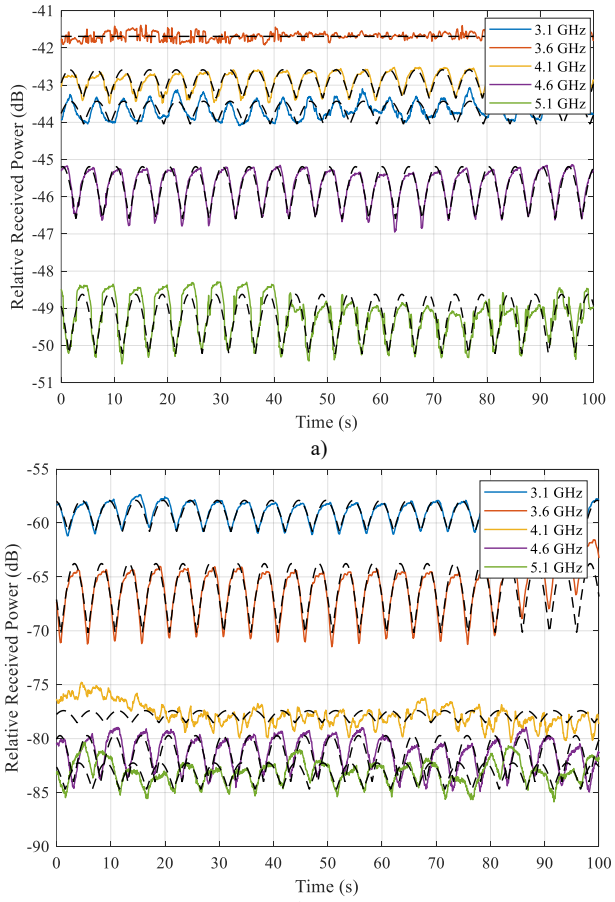

Fig. 4. Relative received power (P_{rel}) as a function of time for different frequencies; a) Case 1, b) Case 2.

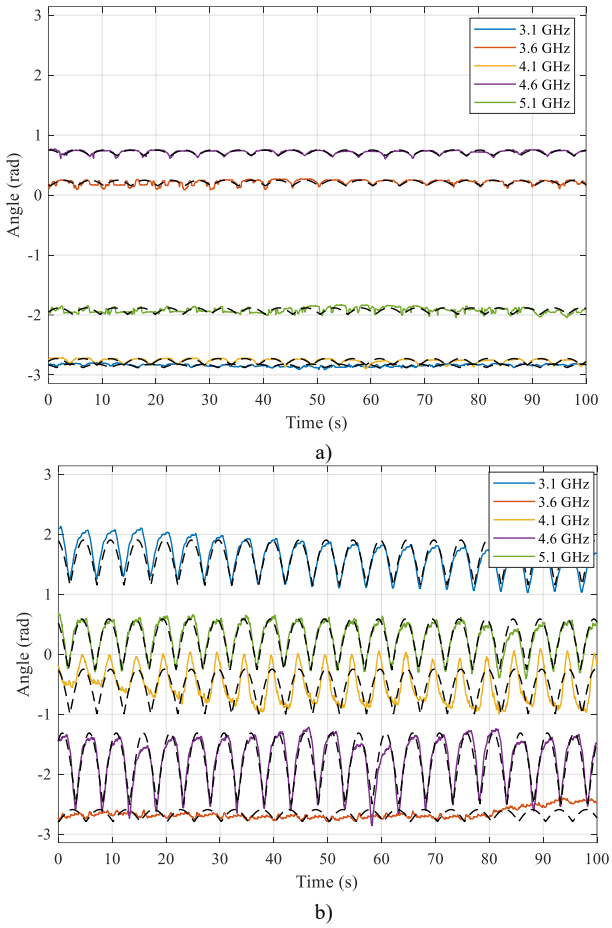

Fig. 5. Phase (radians) of the time-varying transfer function $T(f, t)$: a) Case 1, b) Case 2.

TABLE III
PARAMETERS OF THE ABSOLUTE VALUE OF THE COSINE FOR RELATIVE RECEIVED POWER (P_{REL})

	Case 1				
	3.1 GHz	3.6 GHz	4.1 GHz	4.6 GHz	5.1 GHz
A	-44,05	-41,69	-43,35	-46,60	-50,23
B	0,62	0,00	0,77	1,41	1,61
C	0,20	0,21	0,20	0,20	0,20
D	2,06	1,53	2,14	2,97	0,64
	Case 2				
	3.1 GHz	3.6 GHz	4.1 GHz	4.6 GHz	5.1 GHz
A	-60,80	-70,22	-78,53	-84,03	-84,70
B	2,90	6,46	1,13	4,31	2,45
C	0,20	0,20	0,20	0,20	0,20
D	3,38	1,07	2,33	2,74	3,70

TABLE IV
PARAMETERS OF THE ABSOLUTE VALUE OF THE COSINE FOR THE PHASE OF THE TRANSMISSION COEFFICIENT S_{21}

	Case 1				
	3.1 GHz	3.6 GHz	4.1 GHz	4.6 GHz	5.1 GHz
A	-2.88	0.15	-2.83	0.66	-1.99
B	0.06	0.09	0.11	0.09	0.11
C	0.20	0.20	0.20	0.20	0.20
D	0.64	1.35	1.19	-0.14	1.92
	Case 2				
	3.1 GHz	3.6 GHz	4.1 GHz	4.6 GHz	5.1 GHz
A	1.14	-2.79	-1.00	-2.51	-0.26
B	0.76	0.20	0.75	1.20	0.85
C	0.20	0.20	0.20	0.20	0.20
D	0.20	1.49	0.21	2.67	0.40

For parameter estimation, the Nelder-Mead optimization was used by minimizing the sum of the square errors (SSE) [26]. As observed, the breathing rate obtained was 0.2 breaths per second, which corresponds to 12 breaths per minute. The A parameter –which denotes the mean P_{rel}– tends to decrease with frequency. This effect is also observed in other studies, where the relative received power decreases with frequency [27]. Considering B parameter (maximum excursion), it is larger for Case 2, since, as already mentioned, in this case the thorax is nearer the IB antenna, leading to a large excursion of the P_{rel}.

It should be also noted that for Case 1, f=3.6 GHz, almost no oscillations were observed in P_{rel}. This may be due to a displacement of the IB antenna during measurements because of the natural movement of the internal organs. Such displacement could lead to a mismatch on polarization, and consequently in the received power.

2) Phase

Figure 5 depicts the phase of the transfer function, T(f,t), for the five frequencies considered in this study. As in the previous case, the behaviour of the phase with time is oscillatory as well. Again, the same models as for P_{rel} were applied. The best model for the phase resulted to be the absolute value of the cosine, and it is also plotted in Fig. 5 in dashed line. Table IV shows the parameters of the model, which have been obtained applying a nonlinear least square (NLLS) optimization approach by minimizing the SSE [28]. Again, the breathing rate corresponds to 12 breaths per minute. As for P_{rel}, the variation of the phase with time is larger for Case 2, and consequently the B parameter is larger.

IV. Discussion

As directly derived from Fig. 4, the relative power received at the on-body node varies oscillatorily due to the breathing process. According to our *in vivo* measurements, the excursion of such oscillation mainly depends on two factors: 1) the proximity of the in-body node to the thoratic cage, since it is more pronounced for Case 2 configuration (see Fig.1b); 2) the frequency, since relative received power tends to decrease with the increment of frequency.

Looking at the oscillating behaviour of the received power in Case 2 (worst case), the maximum excursion (B parameter) ranges from 1.1 up to 6.5 decibels. These variations of the received power can have direct implications on real applications, such as localization of WCE [29] or physical layer security for pacemakers [30]. Those applications rely on the estimation of distance between implanted and OB nodes via the their path loss models. Considering the abdominal scenario, the variation per centimeter given by the path loss model is around 6 to 8 dB/cm (depending on using simulations, phantom measurements or *in vivo* measurements) [17]. In case of the chest area, the variation was found to be about 5 dB/cm [18]. This means that a variation of 6.5 decibels due to breathing can lead to a misestimation of the distance between transmitter and receiver even larger than 1 cm, leading to important errors in final applications. Hence, further research is needed in order to know the internal physiological and EM phenomena that give rise to these variations and assuring thus the correct operation of wireless implanted devices.

V. Conclusions

This work analyses the influence of the breathing process in the UWB propagation channel for implanted devices. This analysis has been accomplished by means of CW *in vivo* measurements performed in two different positions, in order to evaluate the influence of the proximity of the thorax to the implanted device. Results showed that both the relative received power (derived from the time-varying transfer function) and its phase exhibit an oscillatory process with time, which can be modelled by an absolute value of the cosine function. Model parameters have been reported so breathing can be replicated when emulating the radio interface of this kind of devices.

References

[1] R. Chávez-Santiago, I. Balasingham, and J. Bergsland, "Ultrawideband technology in medicine: A survey," *J. Electr. Comput. Eng.*, vol. 2012, 2012.

[2] E. Chow, M. Morris, and P. Irazoqui, "Implantable RF Medical Devices: The Benefits of High-Speed Communication and Much Greater Communication Distances in Biomedical Applications," *IEEE Microw. Mag.*, vol. 14, no. 4, pp. 64–73, Jun. 2013.

[3] M. R. Yuce and T. Dissanayake, "Easy-to-Swallow Wireless Telemetry," *IEEE Microw. Mag.*, vol. 13, no. 6, pp. 90–101, Sep. 2012.

[4] M. Waqialla, R. Alshammari, and M. I. Razzak, "An ontology for remote monitoring of cardiac implantable electronic devices," in *2015 International Conference on Computer, Communications, and Control Technology (I4CT)*, 2015, pp. 520–523.

[5] A. Stango, K. Y. Yazdandoost, F. Negro, and D. Farina, "Characterization of In-Body to On-Body Wireless Radio Frequency Link for Upper Limb Prostheses," *PLoS One*, vol. 11, no. 10, p. e0164987, Oct. 2016.

[6] G. Pan and L. Wang, "Swallowable Wireless Capsule Endoscopy: Progress and Technical Challenges," *Gastroenterol. Res. Pract.*, vol. 2012, pp. 1–9, 2012.

[7] M. Patel and J. Wang, "Applications, challenges, and prospective in emerging body area networking technologies," *IEEE Wirel. Commun.*, vol. 17, no. 1, pp. 80–88, Feb. 2010.

[8] R. Chavez-Santiago *et al.*, "Experimental Path Loss Models for In-Body Communications within 2.36-2.5 GHz.," *IEEE J. Biomed. Heal. informatics*, vol. 19, no. 3, pp. 930–937, Apr. 2015.

[9] R. de Francisco and A. Pandharipande, "Spectrum occupancy in the 2.36–2.4 GHZ band: Measurements and analysis," in *2010 European Wireless Conference (EW)*, 2010, pp. 231–237.

[10] R. Chávez-Santiago, I. Balasingham, and J. Bergsland, "Ultrawideband Technology in Medicine: A Survey," *J. Electr. Comput. Eng.*, vol. 2012, pp. 1–9, 2012.

[11] A. Ghildiyal, K. Amara, R. D. Molin, B. Godara, A. Amara, and R. K. Shevgaonkar, "UWB for in-body medical implants: A viable option," in *2010 IEEE International Conference on Ultra-Wideband*, 2010, pp. 1–4.

[12] C. Gabriel, "Compilation of the Dielectric Properties of Body Tissues at RF and Microwave Frequencies.," Jan. 1996.

[13] A. Fornes-Leal *et al.*, "Dielectric Characterization of in Vivo Abdominal and Thoracic Tissues in the 0.5-26.5 GHz Frequency Band for Wireless Body Area Networks," *IEEE Access*, 2019.

[14] C. Garcia-Pardo *et al.*, "Ultrawideband Technology for Medical In-Body Sensor Networks: An Overview of the Human Body as a Propagation Medium, Phantoms, and Approaches for Propagation Analysis," *IEEE Antennas Propag. Mag.*, 2018.

[15] C. Garcia-Pardo *et al.*, "Experimental ultra wideband path loss models for implant communications," in *IEEE International Symposium on Personal, Indoor and Mobile Radio Communications, PIMRC*, 2016.

[16] P. Bose, A. Khaleghi, M. Albatat, J. Bergsland, and I. Balasingham, "RF Channel Modeling for Implant-to-Implant Communication and Implant to Subcutaneous Implant Communication for Future Leadless Cardiac Pacemakers," *IEEE Trans. Biomed. Eng.*, vol. 65, no. 12, pp. 2798–2807, Dec. 2018.

[17] S. Perez-Simbor, C. Andreu, C. Garcia-Pardo, M. Frasson, and N. Cardona, "UWB Path Loss Models for Ingestible Devices," *IEEE Trans. Antennas Propag.*, vol. 67, no. 8, pp. 5025–5034, Aug. 2019.

[18] A. Khaleghi, R. Chávez-Santiago, and I. Balasingham, "Ultra-wideband statistical propagation channel model for implant sensors in the human chest," *IET Microwaves, Antennas Propag.*, vol. 5, no. 15, p. 1805, 2011.

[19] R. G. Garcia-Serna, C. Garcia-Pardo, J. M. Molina-Garcia-Pardo, L. Juan-Llacer, and N. Cardona, "Doppler Characterization in Ultra Wideband BAN Channels during Breathing," *IEEE Trans. Antennas Propag.*, vol. 68, no. 2, pp. 1066–1073, Feb. 2020.

[20] A. A. Serra, P. Nepa, G. Manara, G. Corsini, and J. L. Volakis, "A single on-body antenna as a sensor for cardiopulmonary monitoring," *IEEE Antennas Wirel. Propag. Lett.*, vol. 9, pp. 930–933, 2010.

[21] M. O. Munoz, R. Foster, and Y. Hao, "Exploring physiological parameters in dynamic WBAN channels," *IEEE Trans. Antennas Propag.*, vol. 62, no. 10, pp. 5268–5281, Oct. 2014.

[22] D. Fan *et al.*, "Breathing rhythm analysis in body centric networks," *IEEE Access*, vol. 6, pp. 32507–32513, Jun. 2018.

[23] P. Leelatien, K. Ito, K. Saito, M. Sharma, and A. Alomainy, "Channel Characteristics and Wireless Telemetry Performance of Transplanted Organ Monitoring System Using Ultrawideband Communication," *IEEE J. Electromagn. RF Microwaves Med. Biol.*, vol. 2, no. 2, pp. 94–101, Jun. 2018.

[24] C. Andreu, C. Garcia-Pardo, A. Fornes-Leal, M. Cabedo-Fabrés, and N. Cardona, "UWB In-Body Channel Performance by Using a Direct Antenna Designing Procedure," in *2017 11th European Conference on Antennas and Propagation (EuCAP)*, 2017, pp. 1–4.

[25] E. Miralles, C. Andreu, M. Cabedo-Fabrés, M. Ferrando-Bataller, and J. F. Monserrat, "UWB On-body Slotted Patch Antennas for In-Body Communications," in *2017 11th European Conference on Antennas and Propagation (EuCAP)*, 2017, pp. 1–4.

[26] J. C. Lagarias, J. A. Reeds, M. H. Wright, and P. E. Wright, "Convergence properties of the Nelder-Mead simplex method in low dimensions," *SIAM J. Optim.*, vol. 9, no. 1, pp. 112–147, Jan. 1998.

[27] P. A. Floor *et al.*, "In-Body to On-Body Ultrawideband Propagation Model Derived From Measurements in Living Animals," *IEEE J. Biomed. Heal. Informatics*, vol. 19, no. 3, pp. 938–948, May 2015.

[28] D. W. Marquardt, "An Algorithm for Least-Squares Estimation of Nonlinear Parameters," *J. Soc. Ind. Appl. Math.*, vol. 11, no. 2, pp. 431–441, Jun. 1963.

[29] C. Garcia-Pardo, M. Barbi, S. Perez-Simbor, and N. Cardona, "UWB channel characterization for wireless capsule endoscopy localization," in *2020 IEEE International Conference on Communications Workshops, ICC Workshops 2020 - Proceedings*, 2020.

[30] M. F. Awan, S. Perez-Simbor, C. Garcia-Pardo, K. Kansanen, and N. Cardona, "Experimental Phantom-Based Security Analysis for Next-Generation Leadless Cardiac Pacemakers," *Sensors*, Dec. 2018.